

Supplementary Information for

**Electronic band contraction induced low temperature methane
activation on metal alloys**

Victor Fung^{1*}, Guoxiang Hu¹, Bobby Sumpter¹

¹*Center for Nanophase Materials and Sciences, Oak Ridge National Laboratory, Oak Ridge, Tennessee 37831, United States*

*E-mail: fungv@ornl.gov Tel.: +1-951-384-5242

S1. Methods

The density functional theory (DFT) calculations were performed using the Vienna ab initio Simulation Package (VASP).^{1, 2} The Perdew-Burke-Ernzerhof (PBE)³ functional form of generalized-gradient approximation (GGA) for electron exchange and correlation energies were used. For validation and the calculation of methane activation, the D3 van der Waals correction was used.⁴ Additional validation was also performed with SCAN+rVV10 as described in the main text.^{5, 6} All calculations were performed with spin polarization. The projector-augmented wave method was used to describe the electron-core interaction^{1, 7} with a kinetic energy cutoff of 450 eV for the surface calculations. A 3×3×1 sampling of Brillouin zone using a Monkhorst-Pack scheme was used for the k-points.⁸ A Gaussian smearing of 0.1 eV was used for the density of states. A vacuum layer of 15 Å was created for the surface slabs; the slab contains a total of four layers, with the bottom two layers of the surface slab fixed in the calculations. The sizes of the surface cell are: (100): 3 x 3, (111): $\sqrt{3} \times \sqrt{3}$, (310): 3 x 1, (331): 1 x 2. The convergence of adsorption energy was tested with respect to the number of layers and found energy differences to be within 0.03 eV. Methane adsorption was tested on a larger number of layers, with the adsorption energy difference between 4 and 6 layers to be less than 20 meV. COHP analysis was performed using LOBSTER.^{9, 10}

The methane absorption energy (E_{ads}) is calculated with the equation $E_{\text{ads}} = E_{\text{surface+CH}_4} - (E_{\text{perfect-surface}} + E_{\text{CH}_4})$ where $E_{\text{surface+CH}_4}$ is the energy of the surface slab with a methane. The energies of E_{CH_4} was computed by placing the adsorbate in a cubic cell with a 15 Å wide vacuum in each direction. The methane absorption energy (E_{act}) is calculated with the equation $E_{\text{act}} = E_{\text{TS}} - E_i$ where E_{TS} is the transition state energy and E_i is the energy of the initial state containing a surface with the methane. The methane dissociation energy (E_{diss}) is calculated with the equation $E_{\text{diss}} = E_f - E_i$ where E_f is the energy of the surface containing the dissociated methane and E_i is the energy of the surface containing the methane. Geometric relaxations were performed with a force convergence of 0.02 eV/Å. Transition states (TS) were found with the nudged elastic band (NEB)¹¹ method using a force convergence criterion of 0.05 eV/Å. The free energy for the profile of methane activation was obtained using the relation $G = H + ZPE - T^*S$ where ZPE is the zero-point energy. The ZPE and entropy of the adsorbed species are obtained from DFT vibrational frequencies and the JANAF tables are referenced for gas phase methane.

Charge densities and isosurfaces were visualized using VESTA.¹² The isosurfaces were plotted with an isosurface level of 0.001 e.

S2. Adsorption energies of methane

Table S1. PBE Adsorption energies of methane on single atom alloys in Cu

Element	Cu(100) (η -H,H)	Cu(111) (η -H,H)	Cu(310) (η -H,H,H)	Cu(331) (η -H,H,H)	Cu(331) (η -H,H)
Ti	-0.249 (eV)	-0.231 (eV)	-0.371 (eV)	-0.392 (eV)	-0.330 (eV)
V	-0.220	-0.150	-0.250	-0.249	-0.273
Cr	-0.074	-0.060	-0.156	-0.118	-0.144
Mn	-0.027	-0.025	-0.074	-0.058	-0.059
Fe	-0.084	-0.022	-0.096	-0.054	-0.063
Co	-0.021	-0.022	-0.019	-0.175	-0.175
Ni	-0.018	-0.022	-0.167	-0.073	-0.064
(pure) Cu	-0.014	-0.014	-0.026	-0.018	-0.014
Zn	-0.015	-0.013	-0.011	-0.017	-0.004
Zr	-0.305	-0.327	-0.400	-0.400	-0.333
Nb	-0.320	-0.266	-0.369	-0.398	-0.366
Mo	-0.228	-0.190	-0.205	-0.279	-0.281
Tc	-0.165	-0.109	-0.151	-0.189	-0.188
Ru	-0.151	-0.089	-0.241	-0.219	-0.219
Rh	-0.049	-0.032	-0.118	-0.144	-0.131
Pd	-0.022	-0.019	-0.040	-0.030	-0.047
Ag	-0.017	-0.018	-0.029	-0.024	-0.018
Cd	-0.013	-0.016	-0.019	-0.020	-0.023
Hf	-0.281	-0.283	-0.397	-0.389	-0.320
Ta	-0.261	-0.198	-0.404	-0.376	-0.345
W	-0.231	-0.104	-0.330	-0.287	-0.291
Re	-0.179	-0.050	-0.232	-0.241	-0.171
Os	-0.094	-0.030	-0.256	-0.200	-0.157
Ir	-0.019	-0.022	-0.087	-0.087	-0.079
Pt	-0.017	-0.015	-0.016	-0.010	-0.009
Au	-0.014	-0.016	-0.016	-0.012	-0.006
Hg	0.006	-0.012	-0.013	-0.003	0.027

Table S2. PBE Adsorption energies of methane on intermetallic Cu₅Zr

	Cu ₅ Zr(100)	Cu ₅ Zr(110)	Cu ₅ Zr(111)
E _{ads} (eV)	-0.215	-0.231	-0.213
C-M distance (Å)	2.834	2.836	2.834
C-H distance (Å)	1.110	1.113	1.111

S3. Methane activation energies

Table S3. PBE+D3 Adsorption, activation, and dissociation energies for methane dissociation

Surface	E _{ads} (eV)	E _{act} (eV)	E _{diss} (eV)
Ti/Cu(100)	-0.56	0.56	0.21
V/Cu(100)	-0.54	0.78	0.45
Cr/Cu(100)	-0.35	1.18	0.53
Mn/Cu(100)	-0.12	0.83	0.33
Fe/Cu(100)	-0.52	0.33	0.34
Co/Cu(100)	-0.43	0.38	0.20
Ni/Cu(100)	-0.30	0.67	0.41
Cu/Cu(100)	-0.25	1.39	0.84
Zr/Cu(100)	-0.56	0.59	0.12
Nb/Cu(100)	-0.59	0.44	0.09
Mo/Cu(100)	-0.54	0.43	0.08
Tc/Cu(100)	-0.50	0.35	-0.01
Ru/Cu(100)	-0.49	0.35	0.10
Rh/Cu(100)	-0.35	0.51	0.26
Pd/Cu(100)	-0.24	1.07	0.75
Ag/Cu(100)	-0.18	1.85	1.16
Hf/Cu(100)	-0.55	0.51	-0.08
Ta/Cu(100)	-0.58	0.36	-0.31
W/Cu(100)	-0.58	0.26	-0.36
Re/Cu(100)	-0.54	0.17	-0.36
Os/Cu(100)	-0.45	0.10	-0.36
Ir/Cu(100)	-0.26	0.21	-0.23
Pt/Cu(100)	-0.22	0.78	0.33
Au/Cu(100)	-0.18	1.68	0.86
Ti/Cu(331)	-0.67	0.50	0.01
V/Cu(331)	-0.51	0.53	-0.23
Cr/Cu(331)	-0.35	0.83	0.38
Mn/Cu(331)	-0.27	0.89	0.38
Fe/Cu(331)	-0.33	0.54	0.13

Co/Cu(331)	-0.37	0.13	-0.06
Ni/Cu(331)	-0.32	0.50	0.23
Cu/Cu(331)	-0.25	1.20	0.37
Zr/Cu(331)	-0.62	0.60	-0.02
Nb/Cu(331)	-0.65	0.30	-0.27
Mo/Cu(331)	-0.48	0.25	-0.20
Tc/Cu(331)	-0.39	0.22	-0.20
Ru/Cu(331)	-0.36	0.14	0.30
Rh/Cu(331)	-0.30	0.35	0.13
Pd/Cu(331)	-0.22	0.93	0.65
Ag/Cu(331)	-0.13	1.67	1.05
Hf/Cu(331)	-0.63	0.50	-0.23
Ta/Cu(331)	-0.64	0.20	-0.57
W/Cu(331)	-0.53	0.03	-0.68
Re/Cu(331)	-0.36	-0.06	-0.65
Os/Cu(331)	-0.31	-0.13	-0.71
Ir/Cu(331)	-0.23	0.03	-0.39
Pt/Cu(331)	-0.16	0.57	0.19
Au/Cu(331)	-0.10	1.47	0.85

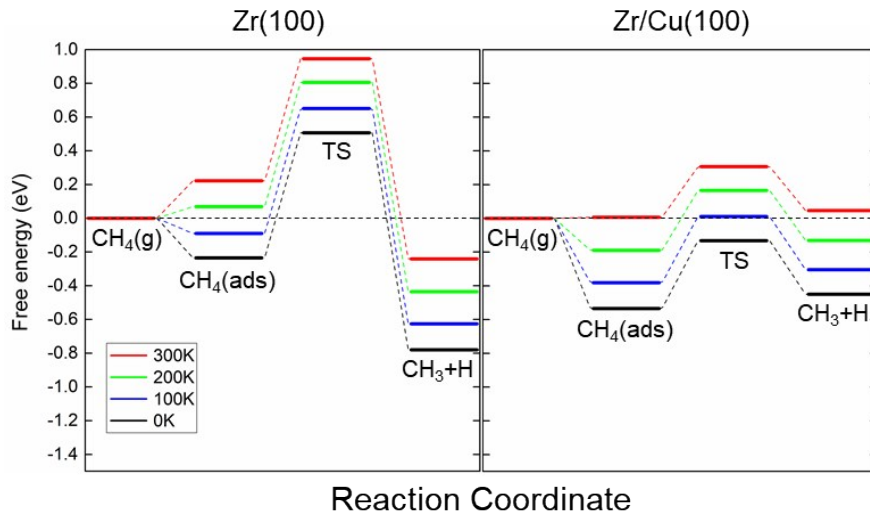


Figure S1: PBE+D3 energy profile comparison of methane dissociation on pure Zr(100) and Zr/Cu(100). The free energies of methane dissociation are shown at various temperatures from 0-300K including zero-point and vibrational contributions to entropy.

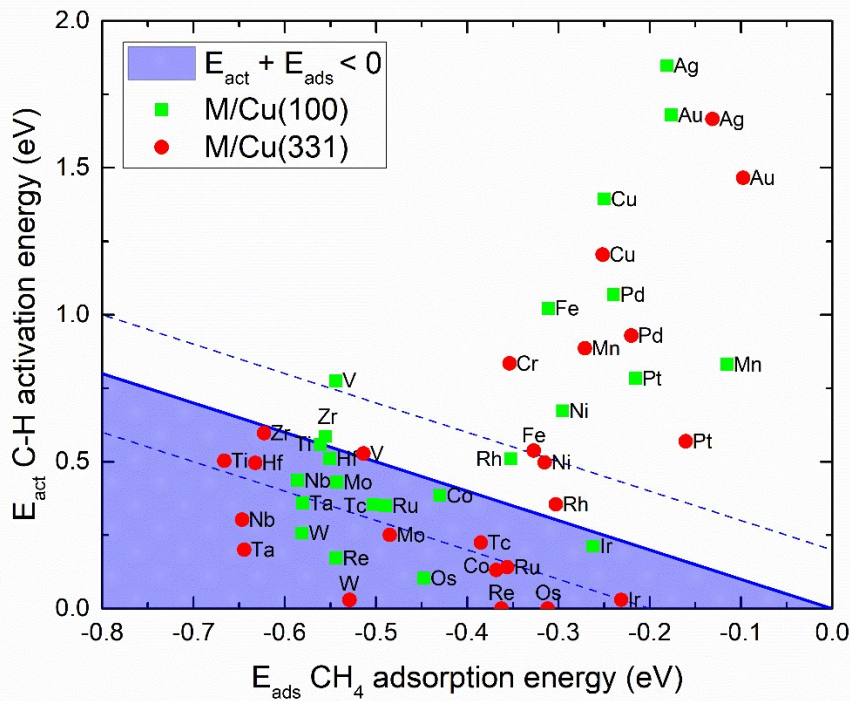


Figure S2: PBE+D3 methane adsorption and activation energies. The region in blue denotes where the desorption energy of methane is higher than its activation barrier, predicting where facile methane activation is likely to occur. The shaded lines show the approximate range of error within 0.2 eV arising from the functional choice.

S4. Parameters for compressed sensing of descriptors

Table S4. Electronic structure parameters for SISSO analysis

Surface	S_{unocc} (states)	p_{unocc} (states)	d_{unocc} (states)	S_{occ} (states)	p_{occ} (states)	d_{occ} (e)	S_{center} (eV)	p_{center} (eV)	d_{center} (eV)	r_s (Å)	r_p (Å)	r_d (Å)
Cu ₅ Zr (100)	0.160	0.297	4.446	0.119	0.139	1.085	-1.580	2.120	0.653	1.265	1.56	0.54
Zr (100)	0.042	0.232	1.562	0.176	0.262	1.787	-2.213	-0.526	-0.312	1.265	1.56	0.54
Ti/Cu (100)	0.083	0.309	4.924	0.089	0.129	1.333	-0.234	2.722	0.958	1.15	1.43	0.28
V/Cu (100)	0.075	0.205	3.042	0.084	0.099	2.388	-0.044	2.087	1.047	1.09	1.34	0.26
Cr/Cu (100)	0.065	0.178	1.478	0.081	0.086	3.181	0.132	2.317	0.940	1.07	1.37	0.25
Mn/Cu (100)	0.059	0.148	3.465	0.073	0.075	1.115	-0.150	2.283	-0.661	0.99	1.23	0.23
Fe/Cu (100)	0.057	0.170	2.509	0.071	0.089	2.557	-1.019	1.792	-0.931	0.95	1.16	0.22
Co/Cu (100)	0.062	0.153	1.446	0.073	0.070	6.072	-0.481	2.151	-0.261	0.92	1.1	0.21
Ni/Cu (100)	0.063	0.159	0.663	0.079	0.076	6.854	-0.581	2.131	-0.626	0.96	1.22	0.195
Cu/Cu (100)	0.064	0.156	0.149	0.084	0.080	3.447	-0.566	2.223	-2.069	0.88	1.16	0.185
Zn/Cu (100)	0.241	0.719	0.100	0.326	0.376	0.133	-1.373	2.121	-6.629	0.82	1.06	0.175
Zr/Cu (100)	0.111	0.484	4.213	0.112	0.160	1.040	-0.162	3.684	1.127	1.265	1.56	0.54
Nb/Cu (100)	0.035	0.065	2.835	0.035	0.029	1.319	0.250	1.862	0.892	1.23	1.53	0.51
Mo/Cu (100)	0.081	0.188	3.119	0.093	0.087	2.694	-0.169	2.101	0.279	1.22	1.5	0.49
Tc/Cu (100)	0.078	0.192	2.383	0.092	0.095	3.073	-0.428	1.991	-0.244	1.16	1.49	0.455
Ru/Cu (100)	0.073	0.163	1.656	0.078	0.077	4.054	-0.392	2.232	-0.462	1.145	1.46	0.45
Rh/Cu (100)	0.072	0.141	1.031	0.078	0.067	5.294	-0.065	2.382	-0.764	1.11	1.41	0.42
Pd/Cu (100)	0.064	0.118	0.410	0.076	0.060	4.728	0.153	2.529	-1.567	1.08	1.37	0.4
Ag/Cu (100)	0.072	0.133	0.097	0.088	0.063	0.366	0.112	2.610	-3.814	1.045	1.33	0.385
Cd/Cu (100)	0.096	0.222	0.034	0.130	0.112	0.044	-0.771	2.597	-8.046	0.985	1.23	0.37
Hf/Cu (100)	0.088	0.264	3.235	0.106	0.120	0.688	-0.938	1.823	1.347	1.3	1.61	0.63
Ta/Cu (100)	0.098	0.329	3.709	0.121	0.148	1.462	-1.354	1.673	0.585	1.25	1.54	0.605
W/Cu (100)	0.083	0.249	3.163	0.104	0.112	2.222	-1.623	1.776	0.192	1.22	1.515	0.59
Re/Cu (100)	0.067	0.191	2.219	0.084	0.088	2.644	-1.542	1.884	-0.138	1.19	1.49	0.565
Os/Cu (100)	0.080	0.225	1.833	0.101	0.105	3.840	-1.585	1.840	-0.549	1.17	1.48	0.543
Ir/Cu (100)	0.083	0.228	1.103	0.112	0.111	4.514	-1.446	2.024	-0.946	1.16	1.468	0.526
Pt/Cu (100)	0.078	0.185	0.496	0.110	0.097	4.148	-1.215	2.206	-1.656	1.24	1.46	0.51

Au/Cu (100)	0.092	0.212	0.168	0.130	0.111	0.962	-1.309	2.270	-3.346	1.21	1.45	0.488
Hg/Cu (100)	0.092	0.241	0.048	0.140	0.127	0.085	-2.033	2.616	-6.308	1.07	1.34	0.475
Zr/Cu (111)	0.128	0.473	3.783	0.101	0.167	0.952	1.047	6.461	1.815	1.265	1.56	0.54
Zr/Cu (331)	0.138	0.527	4.186	0.119	0.127	1.035	0.240	4.643	1.296	1.265	1.56	0.54
Zr/Cu (310)	0.119	0.507	4.360	0.130	0.105	1.059	-0.231	3.467	0.928	1.265	1.56	0.54

The compressed sensing properties described in the main text are listed in table S3. The s, p, d occupied and unoccupied number of states are obtained by integrating the density of states over the energy range 0 to 2 for the unoccupied and -2 to 0 for the occupied. The s, p, d centers were obtained over the entire range of states. The orbital radii were obtained from the literature.¹³

S5. Single atom stability

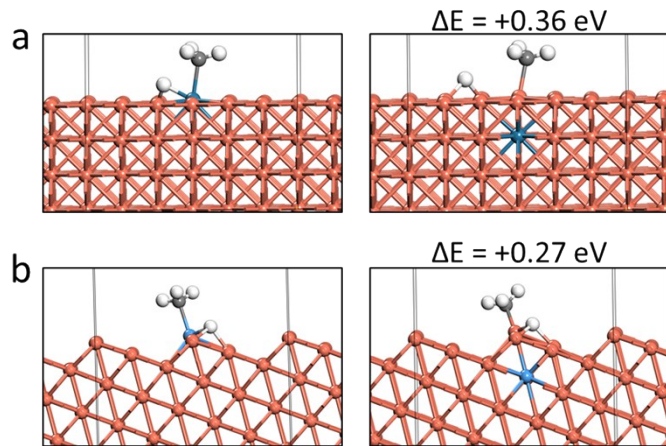


Figure S3: Surface model for segregation energy calculation. Two example surface models of Re/Cu(100) and Ta/Cu(331) for the segregation energy calculation showing the initial state of a dopant on the surface found to a dissociated methane, and a final state where the dopant is in the subsurface layer.

Table S5. Segregation energies in the presence of dissociated methane

Surface	E_{seg} (eV)
Re/Cu(100)	0.27
W/Cu(100)	0.31
Zr/Cu(100)	0.72
Os/Cu(100)	0.29
Ta/Cu(331)	0.36
W/Cu(331)	0.20

S6. Electronic structure of CH₄ on Zr/Cu(100)

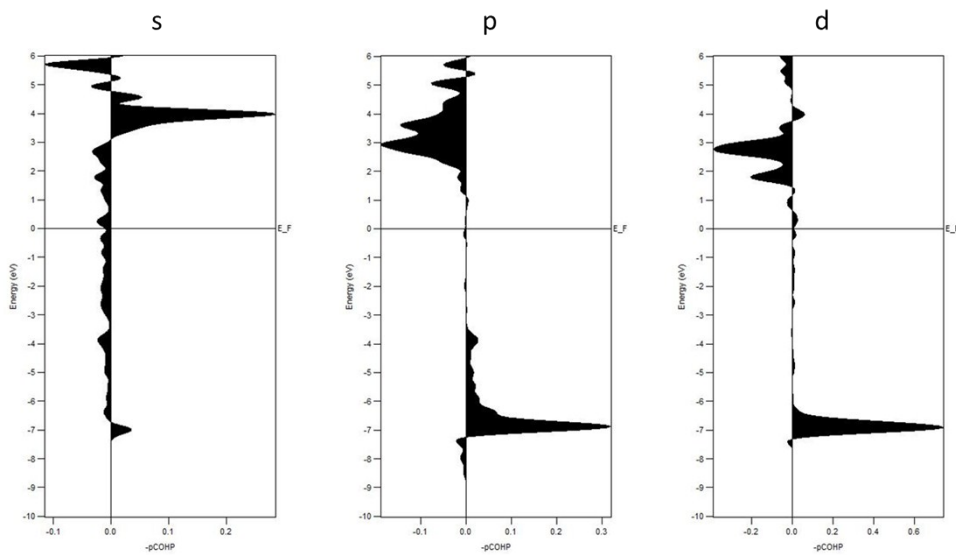


Figure S4: COHP analysis of the C-Zr interaction between CH₄ and Zr/Cu(100). The interaction is separated by the s, p, and d orbital contributions on the Zr atom. Positive values denote bonding and negative values denote antibonding interactions.

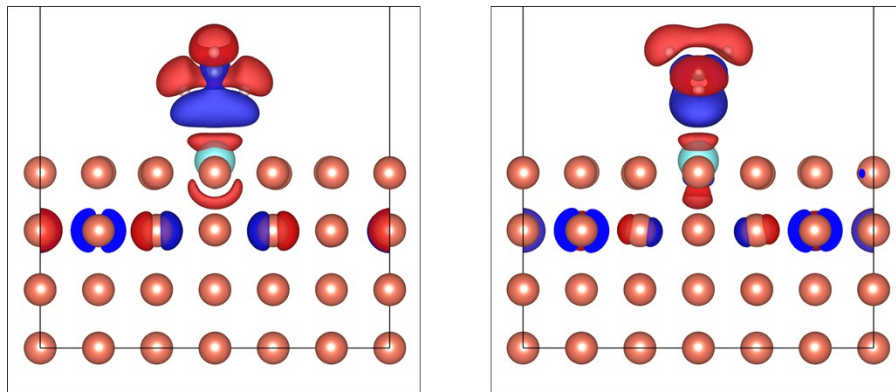


Figure S5: Charge density difference of CH₄ and Zr/Cu(100). Blue values denote increase of charge density and red values denote decrease of charge density. The isosurface value is set to 0.001 e.

References

1. Kresse G., Furthmuller J. Efficiency of Ab-Initio Total Energy Calculations for Metals and Semiconductors Using a Plane-Wave Basis Set. *Comput. Mater. Sci.* **6**, 15-50 (1996).
2. Kresse G., Furthmuller J. Efficient Iterative Schemes for Ab Initio Total-Energy Calculations Using a Plane-Wave Basis Set. *Phys. Rev. B* **54**, 11169-11186 (1996).

3. Perdew J. P., Burke K., Ernzerhof M. Generalized Gradient Approximation Made Simple. *Phys. Rev. Lett.* **77**, 3865-3868 (1996).
4. Grimme S., Antony J., Ehrlich S., Krieg H. A Consistent and Accurate ab Initio Parametrization of Density Functional Dispersion Correction (DFT-D) for the 94 Elements H-Pu. *J. Chem. Phys.* **132**, 154104 (2010).
5. Sun J., Ruzsinszky A., Perdew J. P. Strongly Constrained and Appropriately Normed Semilocal Density Functional. *Phys. Rev. Lett.* **115**, 036402 (2015).
6. Peng H., Yang Z.-H., Perdew J. P., Sun J. Versatile van der Waals Density Functional Based on a Meta-Generalized Gradient Approximation. *Physical Review X* **6**, 041005 (2016).
7. Blöchl P. E. Projector Augmented-Wave Method. *Phys. Rev. B* **50**, 17953-17979 (1994).
8. Monkhorst H. J., Pack J. D. Special Points for Brillouin-Zone Integrations. *Phys. Rev. B* **13**, 5188-5192 (1976).
9. Maintz S., Deringer V. L., Tchougréeff A. L., Dronskowski R. LOBSTER: A Tool to Extract Chemical Bonding from Plane-Wave Based DFT. *J. Comput. Chem.* **37**, 1030-1035 (2016).
10. Deringer V. L., Tchougréeff A. L., Dronskowski R. Crystal Orbital Hamilton Population (COHP) Analysis as Projected from Plane-Wave Basis Sets. *J. Phys. Chem. A* **115**, 5461-5466 (2011).
11. Henkelman G., Uberuaga B. P., Jónsson H. A Climbing Image Nudged Elastic Band Method for Finding Saddle Points And Minimum Energy Paths. *J. Chem. Phys.* **113**, 9901-9904 (2000).
12. Momma K., Izumi F. VESTA 3 for Three-Dimensional Visualization of Crystal, Volumetric and Morphology Data. *J. Appl. Crystallogr.* **44**, 1272-1276 (2011).
13. Zunger A. Systematization of the stable crystal structure of all AB-type binary compounds: A pseudopotential orbital-radii approach. *Phys. Rev. B* **22**, 5839-5872 (1980).